# Planarizing Spalled GaAs(100) Surfaces by MOVPE Growth

Gavin P. Forcade[1], William E. McMahon[2], Nicholas Yoo[3], Anica N. Neumann[2,3], Michelle Young[2], John Goldsmith[2], Sarah Collins[2], Karin Hinzer[1,4], Corinne E. Packard[2,3], Myles A. Steiner[2]

[1] Department of Physics, University of Ottawa, Ottawa, Ontario, Canada

[2] National Renewable Energy Laboratory, Golden, CO, USA

[3] Colorado School of Mines, Golden, CO, USA

[4] SUNLAB, School of Electrical Engineering and Computer Sciences, University of Ottawa, Ottawa, Ontario, Canada

**ABSTRACT:** III-V photovoltaic devices have demonstrated exceptional performance across various applications, with controlled crystal fracturing, known as controlled spalling, emerging as a promising method to reduce costs by enabling substrate reuse. Spalling GaAs(100) substrates, a commonly used substrate in III-V photovoltaics, results in faceted ridges that must be planarized to grow high-quality photovoltaic devices. Here we demonstrate that a GaAs(100) wafer offcut towards $[0\bar{1}1]$ and spalled towards [011] can be efficiently planarized by growing C:GaAs by metal-organic vapor phase epitaxy (MOVPE) on the surface, with up to 95% of the nominally deposited material used to fill the valleys between ridges. We find that reducing the offcut to 2° enhances the planarizing capability of C:GaAs. A surface morphology model indicates that the density of surface dangling bonds significantly influences the growth evolution of undoped GaAs surfaces. In contrast, the model suggests that the effectiveness of C:GaAs as a smoothing layer stems from modifying the atomic surface structure and, consequently, the associated sticking coefficients of the facets, which can alter the evolution of surface morphology. Our findings provide guidelines for the epitaxial planarization of semiconductor surfaces and improve the understanding of MOVPE growth on non-planar surfaces.

KEYWORDS: *MOVPE, MOCVD, substrate reuse, spalling, III-V, GaAs, Carbon tetrachloride, surface planarization, patterned substrate*

## 1. INTRODUCTION

III-V photovoltaics have the highest optical-to-electrical conversion efficiency of any material class, making them an attractive option for applications such as solar photovoltaics,[1,2] waste-heat recovery[3], thermal energy grid storage,[4,5] and power-by-light.[6] III-V photovoltaics dominate space deployments[7] but require cost reductions to penetrate terrestrial markets.[8] Substrate reuse has an enormous potential to reduce III-V photovoltaic costs because substrates account for about a quarter of the cost of high-efficiency solar cells.[8] High-quality substrates are required for device growth[1] but are not generally part of the final device structure, making substrate reuse a cost-saving possibility.

Controlled spalling has the greatest potential for photovoltaic substrate reuse (see Figure 1(a-d) for the reuse process) among the methods proposed so far,[9] because of its high-speed throughput, low capital expenses, minimal chemical hazards, and negligible impact on photovoltaic performance.[10] Controlled spalling consists of mechanically fracturing off the epilayers from the substrate with the help of a stressor layer to control the fracture depth (Figure 1(a)).[9] Ideally, the spalled surfaces of GaAs(100), a common substrate for photovoltaic devices, would be smooth to facilitate the growth of the next photovoltaic devices.[1] Instead, the spalled surfaces consist of a periodic array of ridges with facets oriented on or near natural cleavage directions.[9] These ridges form around the depth directed by the applied stress field as these crystal facets have lower surface energy than the (100) facet. To grow high-quality photovoltaics, the surface needs to be planarized to avoid problems such as parasitic shunts as demonstrated in several references.[1,11,12] This could be done *ex situ* with chemical-mechanical polishing but that proves costly,[9] or by wet chemical etching but there has yet to be a solution that fully planarizes the surface.[11,13] Also, both tend to exacerbate substrate thinning. An alternative approach we investigate here is *in situ* surface smoothing by growing specialized III-V epilayers before cell-layer growth. This method can replenish spalled substrate material but should be done with minimal material and growth times to minimize costs.[8]

There have been promising results for *in situ* smoothing of GaAs surfaces.[1,14–16] Braun et al.[15] planarized 6 μm tall faceted ridges from a GaAs(100) wafer, exfoliated by controlled spalling, by depositing undoped GaAs via hydride vapor phase epitaxy. Although hydride vapor phase epitaxy promises cost reductions for solar photovoltaic growth, most commercial III-V photovoltaics are grown by metal-organic vapor phase epitaxy (MOVPE). Thus, we require a MOVPE planarization solution to achieve substrate reuse in the short term. Schulte et al.[1] grew 2 μm of

Zn:GaInP by MOVPE to partially planarize an acoustically spalled GaAs substrate with initial ridge heights of less than 1 µm. However, growing ternary materials on a patterned surface can spatially vary the composition, causing lattice mismatching[17–19] (see Supporting Information for an example). Kim et al.[14] explored some growth conditions for planarizing 1.5 µm deep valleys, generated by patterned etching, with C:GaAs grown by MOVPE. McMahon et al.[16] planarized 5+ µm tall faceted ridges from a GaAs(100) wafer, exfoliated by controlled spalling, using C:GaAs and Si:GaAs grown by MOVPE and demonstrated that the choice of growth material, surface dopant, along with the offcut and spall directions, have a large impact on surface planarization. Building upon this preliminary work, we find the wafer offcut angle is also crucial for surface planarization.

In this paper, we optimize the planarization process of 5+ µm tall ridges using C:GaAs by MOVPE improving material use such that the amount of growth to achieve planarization is within 5% of the theoretical minimum, given the growth rate and initial surface geometry. We study the growth evolution for varying carbon gas flow rates and GaAs(100) wafer offcuts and describe the main smoothing mechanisms involved.

## 2. EXPERIMENTAL SECTION

Standard single-junction GaAs solar cells were grown on epi-ready 2” (100)GaAs wafers with 6°A, 6°B, 4°B, and 2°B offcuts. These substrates were spalled towards [011] forming A-faceted ridges, defined here as an A spall, and then growth conditions were varied to determine their impact on planarizing the spalled surface. The A spalls formed ridges that ran parallel to the (111)A "Ga-terminated" atomic steps from an A offcut as depicted in Figure 1(e,f). For the spalling conditions used in this study, these spalls formed approximately 5 µm tall {*h*11}A faceted ridges. When a B offcut wafer was A spalled, the "As terminated" (111)B atomic steps from the offcut ran perpendicular to the (111)A facets forming the sides of the ridges, as shown in Figure 1(g).

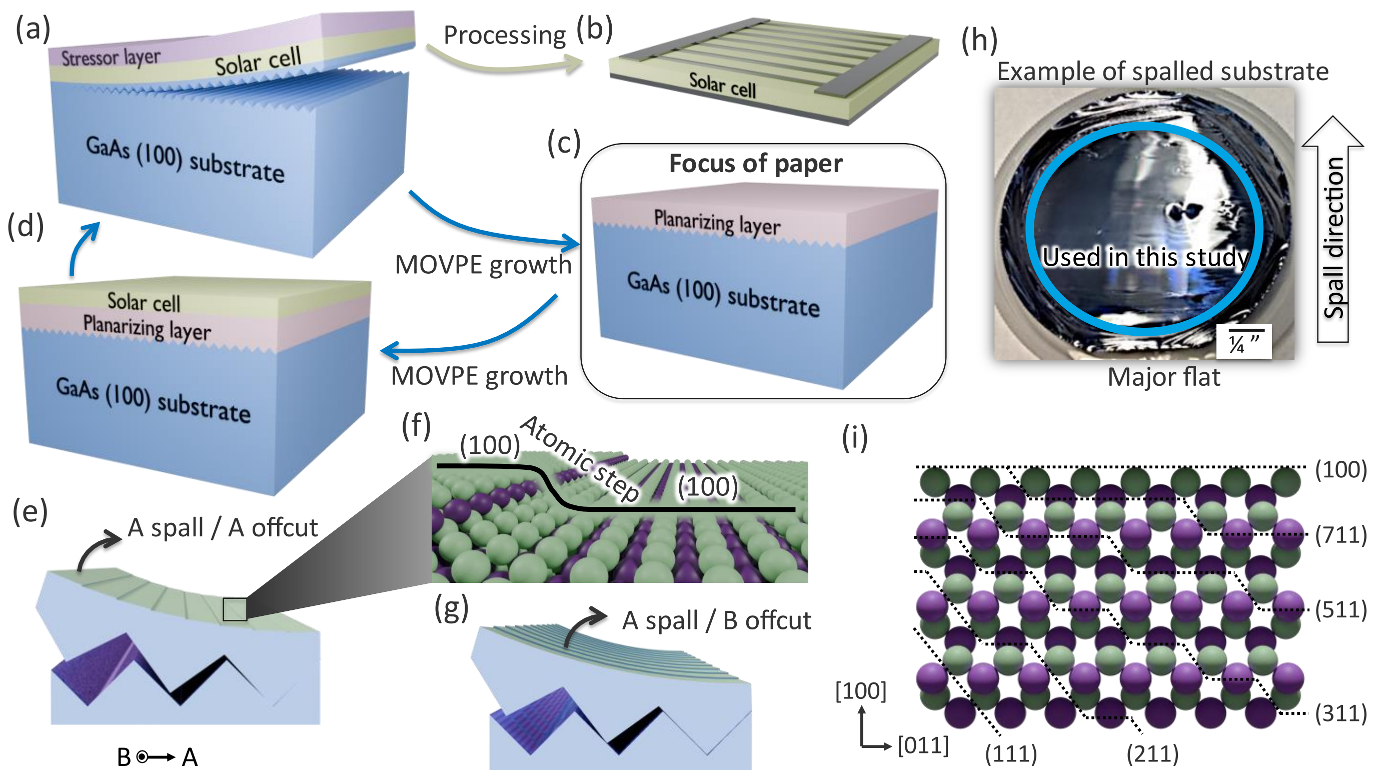


**Figure 1.** GaAs(100) substrate reuse process via controlled spalling. (a) Schematic diagram of the controlled spalling technique with the crack propagating near the GaAs (100) substrate surface causing a faceted surface. (b) The solar cell can be processed into devices. The spalled substrate can be reused by first (c) planarizing the surface, then (d) growing another high-quality solar cell and (a) re-spalling. (e) **S**chematic diagram of an A spall on an A offcut wafer. The lines on the light green surface represent (111)A atomic steps between two (100) terraces, as depicted in (f), with the purple spheres representing Ga atoms. The spalled purple surface is a facet comprising dense atomic steps. (g) Schematic diagram of an A spall on a B offcut wafer with atomic steps perpendicular to the ones in (e). These atomic steps can be represented by (f) but with the purple atoms being As. (h) Top view photograph of a spalled 2” GaAs(100) wafer, spalled starting at the major flat. (i) Illustration of the atomic arrangements between the (100) and (111) surfaces. For A-type facets, purple and green spheres in (i) represent Ga and As atoms, respectively, and vice-versa for B-type facets.

All spalled wafers were processed using the controlled spalling technique with a stressor layer made of Ni alloyed with P and a roller to peel off the top surface,[9] as illustrated in Figure 1(a). The stressor layer was deposited by electrodeposition in a bath composed of 0.6 M nickel(II) chloride hexahydrate and 5 mM phosphoric acid. The deposition was done at a fixed current density of 15.6 mA/cm$^2$ for 18 to 30 minutes to tune the spall depth. After electrodeposition, the wafer was laminated with tape, and an external force was applied to the wafer surface using a linearly actuated motor to initiate and propagate the spalling fracture. Other relevant procedures followed that of ref.[9] A top-view photograph of a GaAs(100) offcut wafer, exfoliated by controlled spalling is shown in Figure 1(h). The interior part of the spalled wafer, demarcated by the thick blue line, was used to investigate planarizing growth, ensuring a consistent baseline for each experiment. Most samples were loaded directly into the reactor without preparation, except for one sample etched with $H_2SO_4$:$H_2O$:$H_2O_2$ at a bottle strength volumetric ratio of 8:1:1 for 13.5 minutes at 30°C which followed the procedure of ref.[13] to reduce the ridge height.

### 1. Growth Details.

III-V epi-layers were grown in a custom-built atmospheric-pressure MOVPE reactor, using trimethylgallium, triethylgallium, trimethylaluminium, trimethylindium, $AsH_3$, $PH_3$, $CCl_4$, $Si_2H_6$, $H_2Se$, and diethylzinc as sources. The $CCl_4$ was mixed with purified hydrogen in a dilution line. Each planarization growth included spalled and as-received wafer samples with identical offcuts and were cleaved to be no less than 1 cm × 1 cm. The planarizing growth consisted of an initial 0.1 μm undoped GaAs layer with a subsequent 10-layer superlattice composed of 1 μm C:GaAs planarizing layers and 0.2 μm C:$Al_{0.43}Ga_{0.57}As$ marker layers. All stated layer thicknesses correspond to the nominal values expected for undoped GaAs grown on a planar GaAs(100) offcut wafer. Cross-sectional scanning electron microscopy images were acquired to characterize the growth evolution with a Hitachi S-4800 operating at 3 kV and a 7μA beam current. The cross-sections were prepared by cleaving along {110} planes, perpendicular to the spalled ridges.

The $CCl_4$ gas flow rate was varied from 0.0 to 0.1 sccm; the highest flow rate of 0.1 sccm can dope C:GaAs at $10^{19}$ cm$^{-3}$ (p-type) in this MOVPE reactor, for typical growth conditions. Four recipes were investigated: the recipe from McMahon et al.[16] (M), the best planarizing recipe from Kim et al.[20] (K), and two variations ($K_{slow}$ & $K_{fast}$) around recipe K. Growth parameters for the recipes are provided in Table 1. They include nominal growth rates for the corresponding material grown undoped on a planar GaAs(100) offcut substrate. The AlGaAs layers were grown at a V/III ratio of 80 with $CCl_4$ flow rates and growth temperatures identical to the GaAs layers.

**Table 1**. Growth conditions for planarizing epi-layers. *T* is the growth temperature. Recipe M comes from McMahon et al. [16]. Recipe K is the best planarizing recipe extracted from the results given by Kim et al. [20].

| *Recipe* | *T* (°C) | *GaAs growth rate* (μm/h) | *GaAs V/III* | *AlGaAs growth rate* (μm/h) |
|---|---|---|---|---|
| M | 650 | 6 | 17 | 4 |
| $K_{slow}$ | 680 | 3.5 | 17 | 4 |
| K | 680 | 6 | 60 | 4 |
| $K_{fast}$ | 680 | 7 | 60 | 12 |

## 3. RESULTS AND DISCUSSION

### 1. Impact of $CCl_4$ Flow Rate on Planarization.

Increasing the $CCl_4$ gas flow improved the planarization capability of C:GaAs material. Cross-sectional scanning electron microscope images of four A spall/A offcut samples with $CCl_4$ flow rates varying from 0.0-0.1 sccm are shown in Figure 2. Including $CCl_4$ gas improved the valley filling rate of the ~5 μm ridges, reducing the

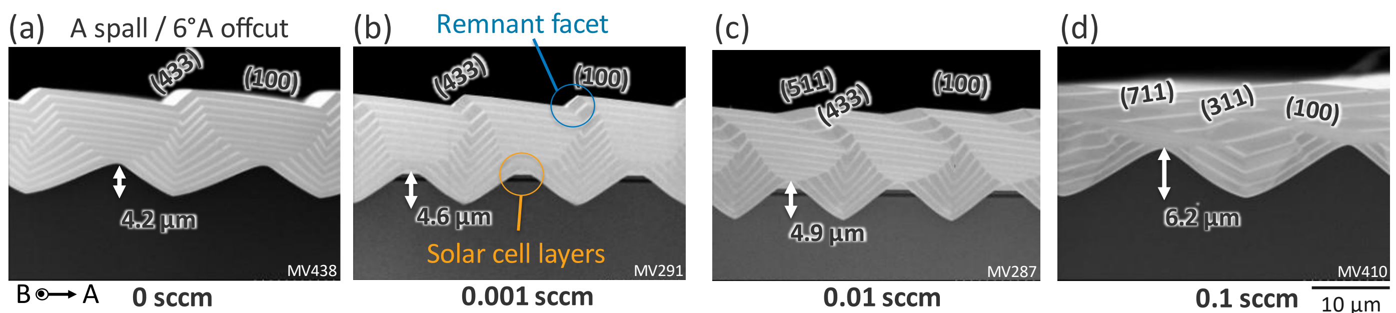


**Figure 2.** C:GaAs grown on A spall/6°A offcut samples. Cross-sectional scanning electron microscope images of spalled substrates with C:GaAs planarizing epi-growth at $CCl_4$ gas flow rates of (a) 0.0 sccm, (b) 0.001 sccm, (c) 0.01 sccm, and (d) 0.1 sccm. These growths utilize the recipe M. The horizontal epilayers at the ridge peaks in (b,c) are solar cell layers pierced by the spalling process. Note: The spall that gave the samples for (b,c) was a preliminary depth-calibration controlled spall, subsequent spalls did not pierce epilayers as shown in (a,d).

nominal growth needed to fill the valley trench from 9 µm (no gas flow) to 4 µm (0.1 sccm).

In Figure 2, we identify the observable crystal facets formed after the valley trenches were filled. Facet emergence depends on the surface morphology, with the fastest-growing facets forming at concave areas and the slowest-growing at convex areas during growth.[21] The (100) crystal plane had the slowest growth rate among the available facets and was further inhibited by $CCl_4$ or its by-products. At large $CCl_4$ flow rates, the highest growth rate facets shifted towards shallower facet angles, from (311)A to (711)A (see Figure 1(i) for a cross-sectional illustration of these atomic surfaces). However, the final surface remained non-planar with remnant facets (Figure 2(b)), which are unfavorable for subsequent solar cell growth.[1] These facets can form when one side of a valley trench is taller than the other; once the trench fills, the extra height of the taller side remains as a remnant facet. Subsequent examples will show that these remnant facets can be avoided with an A spall on a B offcut wafer configuration.

The epi-layer stack at the ridge tips in Figure 2(b,c) was not part of our planarization recipe, and their origins are summarized in the figure caption. These epi-stacks should not affect our planarization growth as the initial 0.1 µm undoped GaAs layer provides a constant starting point before growing our planarizing layers.

## 2. Material Flow Analysis During C:GaAs Epitaxy.

Despite the challenges posed by remnant facets imaged in Figure 2 and illustrated in Figure 3(a), these growths enabled us to evaluate material flow during epitaxy before filling the valley trenches. A consistent material transfer from (100) plateaus to valley regions was observed and is depicted in Figure 3(b). This transfer was evident during at least a portion of each growth cycle, with all instances exhibiting positive valley growth gains relative to conformal growth. We calculated this gain by comparing the measured cross-sectional valley growth area to the nominal cross-sectional growth area, considering the valley width of a planarizing layer as the average between the cladding

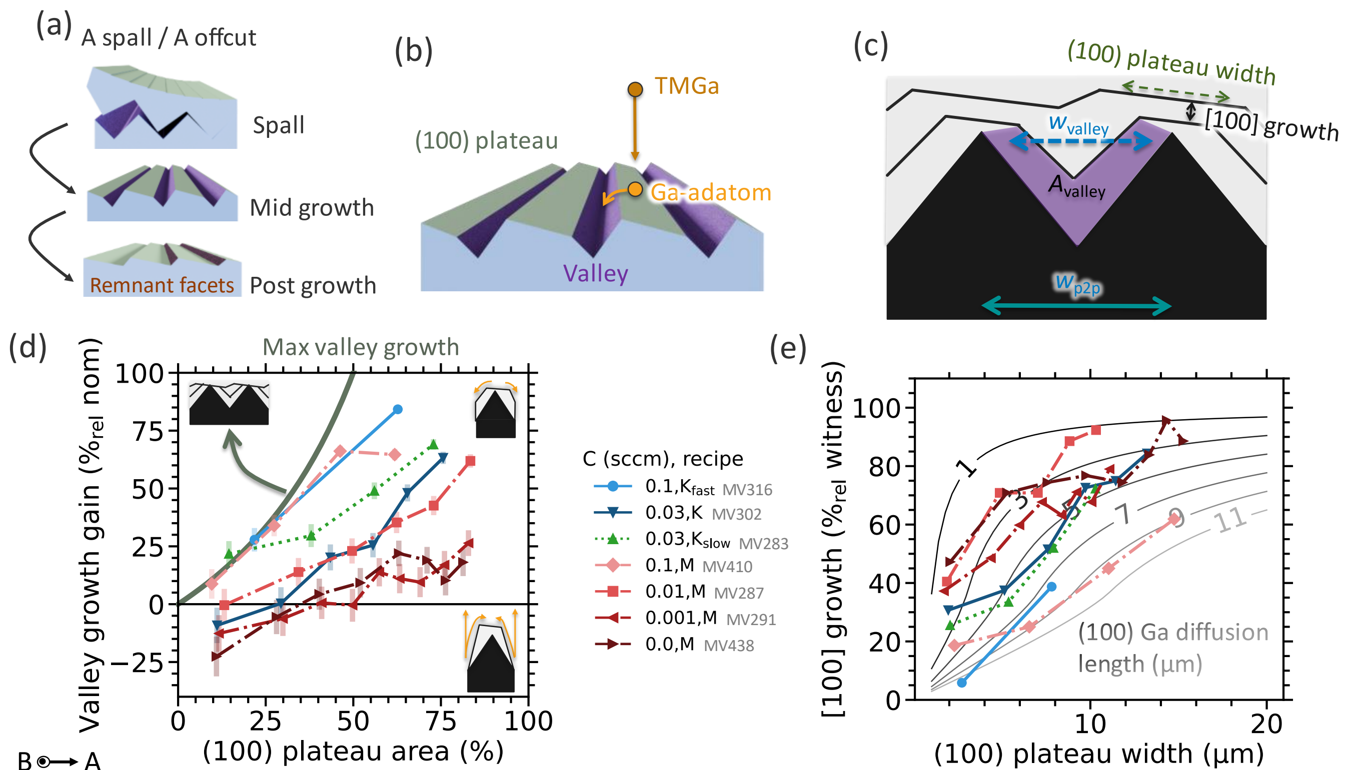


**Figure 3.** Ga-adatom diffusion on (100) surfaces. (a) Schematic diagram showing the growth evolution of the A spall/A offcut samples with the slowest growing crystal facet not perpendicular to the surface normal, causing remnant facets. (b) Schematic illustration of the growth process with diffusion across the (100) plateaus, starting with TMGa precursors that deposit Ga-adatoms on the (100) surface which then diffuses to the valleys. (c) Schematic diagram of C:GaAs grown on A spall/A offcut samples used to define the axis in (d,e). (d) The gain in valley growth relative to the nominal growth on a flat surface $\{(1 - A_{valley}/[w_{valley} \times \text{Nominal growth}]) \times 100\}$ as a function of the (100) plateau horizontal width relative to the periodic structure width $\{(1 - w_{valley}/w_{p2p}) \times 100\}$. The thick green curve represents the maximum valley growth gain. (e) Plotting measured [100] growth on the (100) plateaus relative to the growth on 6°A offcut witness samples as a function of the (100) plateau width. Comparing to simulated curves with the "Adatom diffusion model" detailed in Supporting Information. The error bars in (d) indicate a 50 nm uncertainty in the position of the layer interfaces. Assuming the same uncertainty, error bars for (e) are approximately ±10% absolute but are not shown, to improve the plot's clarity.

marker layer corner edges, as shown in Figure 3(c). We calculated the valley growth gain for each planarizing layer up to the layer that filled the valley trench and plotted the results in Figure 3(d). Comparing the four red curves (recipe M) shows that the valley growth gain increases with $CCl_4$ flow rate.

We find that growth conditions impact the valley growth gain. By comparing the green (recipe $K_{slow}$) and blue (recipe K) triangles in Figure 3d, we demonstrate 71%$_{rel}$ higher average valley growth gain for slower growth rates. We also investigated the optimal growth conditions for C:GaAs as suggested by reference[14] (recipe K), which involves a 30°C higher growth temperature and a V/III ratio that is 3.5 times higher than our standard recipe M. Additional research is required to conclusively determine the impact of these modified growth conditions on planarizing spalled GaAs(100) surfaces.

When employing the highest $CCl_4$ flow rate of 0.1 sccm, we achieved the maximum valley filling gain, marked by the thick green curve in Figure 3(d), for smaller (100) plateau areas. Here, the entirety of the nominally grown material contributed to filling valleys. However, for larger (100) plateaus, we observed a departure from the maximum valley filling, indicating a finite diffusion length of Ga-adatoms across these plateaus.

The diffusion length of Ga-adatoms on (100) surfaces was found to increase with the $CCl_4$ flow rate. This diffusion length was quantified by comparing measured and calculated [100] growth as a function of the (100) plateau width. The data are plotted in color in Figure 3(e), along with modeled black/grey background curves calculated assuming diffusion lengths from 1-11 µm. The measured data come from taking the ratio between the [100] growth on (100) plateaus against flat 6°A offcut witness samples. The calculated values assume a simple Ga-adatom diffusion model based on geometrical considerations (see "Adatom diffusion model" section in Supporting Information for model details). The Ga-adatom diffusion length on (100) surfaces increased with carbon flow, ranging from 3 µm to 8 µm for 0.0 to 0.1 sccm $CCl_4$ flow rates, respectively. These values are about 100 times larger than the Ga-adatom diffusion lengths on crystal facets perpendicular to (111)B during MOVPE growth of undoped GaAs nanowires for growth temperatures less than 470 °C.[22] However, they are of the same order of magnitude as Ga-adatom diffusion lengths on (100) crystal facets during molecular beam epitaxy of undoped GaAs,[23,24] ranging over 0.4-8.0 um depending on the growth conditions and movement direction.

## 3. Impact of B Offcut on Planarization.

Unlike A spall/A offcut samples, the A spall/B offcut configuration suppresses remnant facet formation, thereby facilitating surface planarization. This outcome

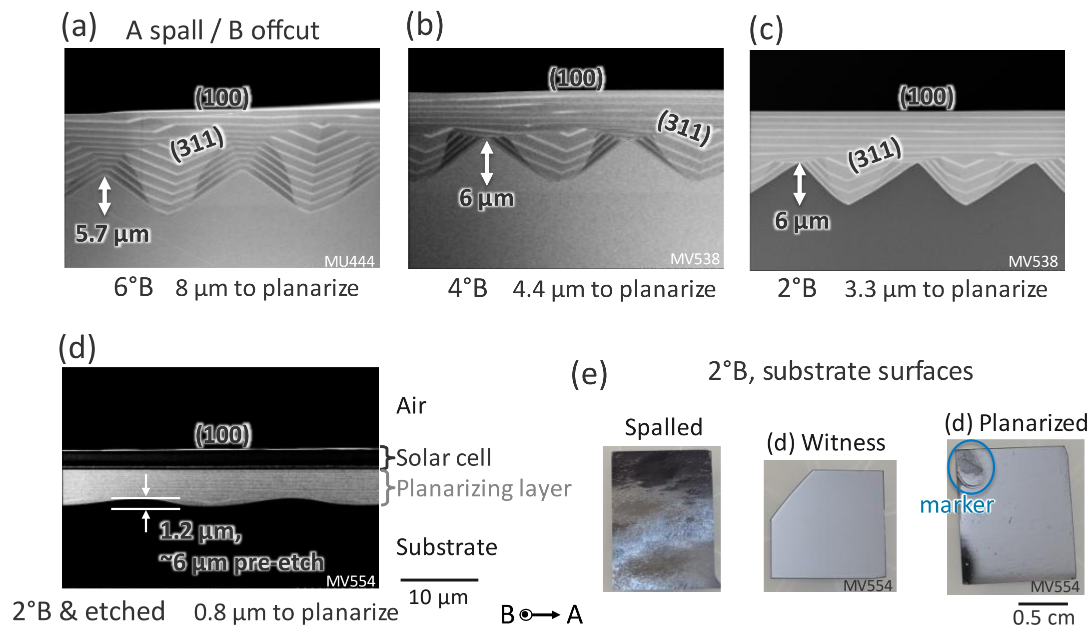


**Figure 4.** C:GaAs grown on A spall/B offcut substrates. Cross-sectional scanning electron microscope images of spalled substrates with C:GaAs planarizing epi-growth for GaAs substrates offcut from (100) towards (a) 6°B, (b) 4°B, and (c,d) 2°B. (d) Using an etching step before planarizing growth, with halved planarizing layer nominal thicknesses. The dark layers above the planarizing layers in (d) comprise a single-junction GaAs solar cell. (e) Top-view photographs of 2°B wafers in their A spalled state, alongside the planarized sample shown in (d) and its corresponding witness sample. All growths use recipe M and are at a $CCl_4$ flow rate of 0.1 sccm.

is visible in the scanning electron microscope images shown in Figure 4(a-d). The growth experiments with C:GaAs, conducted at the highest $CCl_4$ flow rate of 0.1 sccm, demonstrate that smaller B offcuts improve planarization performance. We highlight the effectiveness of the best planarizing growth with the top-view photographs in Figure 4(e), where we compare an as-spalled sample to a planarized sample (same sample as Figure 4(d)) and its corresponding witness sample. In the A spall/B offcut configuration, the two-dimensional surface plateaus that developed at the ridge tops maintained the wafer's original B offcut orientation, as depicted in Figure 5(a). These plateau surfaces were composed of (100) terraces interspersed with (111)B atomic steps.

Reducing the density of (111)B atomic steps decreases the nominal growth of C:GaAs needed to fill the valley trenches, defined as nominal growth to planarize. The (100)2°B surface, with nominally threefold fewer (111)B steps than the (100)6°B surface, required at least two times less nominal growth to fill the valleys for a given ridge height, as illustrated in Figure 5(b). This observation suggests that the (111)B steps have a higher sticking coefficient than the (100) terraces for our growth conditions. Notice that the required growth to planarize samples with 2°B offcuts stays within 30% of the minimum growth to planarize (thick green line).

Incorporating an etching step to partially planarize the spalled surface before the growth phase can reduce the material required to achieve a planar surface by decreasing the initial ridge height. For example, Figure 4(c) and Figure 4(d) depict identical growth conditions and sample offcuts, but the sample in Figure 4(d) which included a planarizing etching step required four times less C:GaAs to achieve a planar surface. In addition to requiring less growth material, adding the etching step reduced the planarization growth time from approximately 33 minutes to 8 minutes.

The initial ridge width influences the quantity of growth required to achieve a planar surface. The material use, defined as the ratio between the minimum and nominal growth needed to planarize a surface with a given initial geometry, as a function of initial ridge width ($w$) is shown in Figure 5(c) for the 2°B experiments. Up to 95% of the nominal material was used to fill the valleys (highest data point in Figure 5(c)), with the remainder either desorbed or deposited on the plateaus. The curve in Figure 5(c) serves as a visual guide and follows the functional form, $0.5/(0.5 + 0.0064w)$. This equation is based on the physical principle that the minimum growth to planarize an initial triangular surface geometry, is 0.5 (slope of the thick green curve in Fig. 5b). The actual required growth (denominator) can be represented by the sum of the ideal case (0.5) and a perturbation ($0.0064w$) resulting from the finite diffusion length of Ga adatoms. Using values from this curve, a spalled sample with a ridge width of 30 µm would require 36% more nominal growth to achieve a planar surface compared to a sample with a 10 µm ridge width, assuming identical ridge heights.

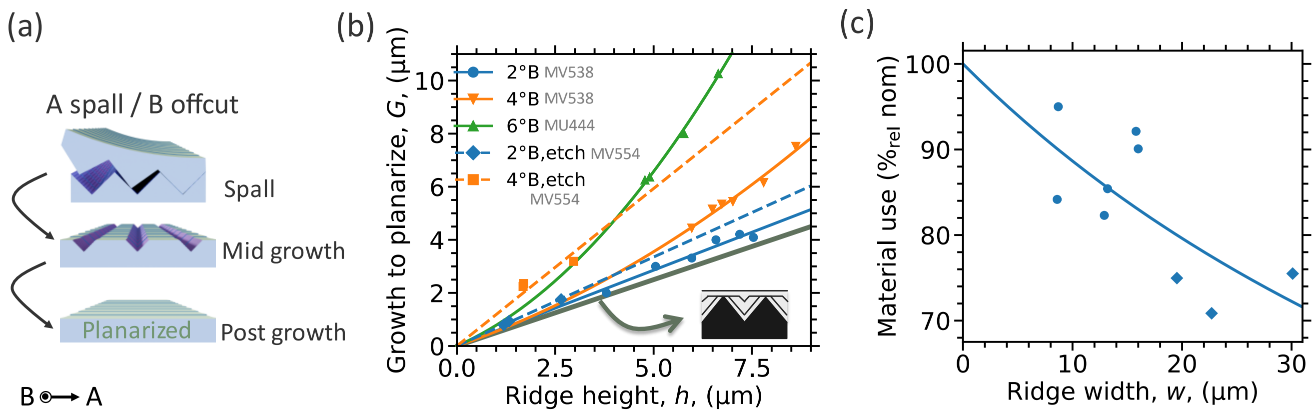


**Figure 5.** Quantifying C:GaAs planarizing capability on A spall/B offcut samples. (a) Schematic diagram of the growth evolution for A spall/B offcut samples where the slowest growing crystal plane is perpendicular to the surface normal. The lines on the planar surface represent atomic steps. (b) Nominal growth required to planarize the spalled surface for a given ridge height. We acquired data over multiple locations on the samples to get a range of ridge heights. The thick green curve represents the best-case scenario where all nominal material is used to planarize the surface. The other curves are quadratic fits to the data to guide the eye. (c) The material used to planarize, defined as the ratio between the minimum and nominal growth to planarize the surface for a given initial surface geometry $\{(0.5/[G/h])\times 100\}$, as a function of the ridge width for 2°B etched and unetched samples. The solid curve in (c) is to guide the eye. The data in (b) and (c) were collected at the same locations. All the growths use recipe M with a 0.1 sccm $CCl_4$ flow rate.

## 4. Modeling Surface Morphology Evolution.

To begin to understand the physical mechanisms that cause our observed growth modes, we simulated the surface morphology evolution during growth with the model from ref.[21] that considers the facet growth rate ($R$) and the diffusion length ($L$), and compared those results to cross-sectional scanning electron microscope images in Figure 6. We used different sets of parameters, $R$ and $L$, for each simulated surface morphology evolution, ensuring they remained constant within each simulation. The model assumes the time ($t$) dependent vertical ($z$) growth is given by:[21]

$$\frac{\partial z}{\partial t} = \sqrt{1+p^2}R(\phi) - \frac{\sqrt{1+p^2}L^2}{2}\left(\frac{\partial^2 R(\phi)}{\partial s^2} - R(0)\frac{d^3 x}{ds^3}\right) \quad (1)$$
$$ds = \sqrt{1+p^2}dx, \qquad p = \frac{\partial z}{\partial x}$$

where $x$ is perpendicular to the wafer's surface normal and $\phi$ is the angle deviated from the wafer's surface normal. Although an atomic model combining fluid dynamics with kinetic Monte-Carlo simulations can be more robust,[25,26] we chose the analytical model from ref.[21] due to its simplicity, since it only has two free parameters, L and $R(\phi)$. Though it cannot be used to accurately extract physical parameters, the model reproduces surface morphology evolution allowing us to postulate dominating growth mechanisms on the faceted surfaces. The modeled results in Figures 6(d-f) show equally time-spaced snapshots of the surface morphology with the colored curves. Note that the model disregards growth extending into the third dimension (into the page). A detailed description of the model is given in the Supporting Information; here we summarize the main physical inputs.

Following the approach from reference,[27] we assume the facet growth rate ($R$) at an angle $\theta$ from (100) is given by:

$$R(\theta) \propto C_0 D_i(\theta)[1 + C_1 S(\theta) + C_2 W(\theta)] + C_3\cos(\phi) \quad (2)$$

where $C_j$ with $j = 0,1,2,3$ are weighting factors and $D_i(\theta)$ with $i = 0,1$ represents the unreconstructed

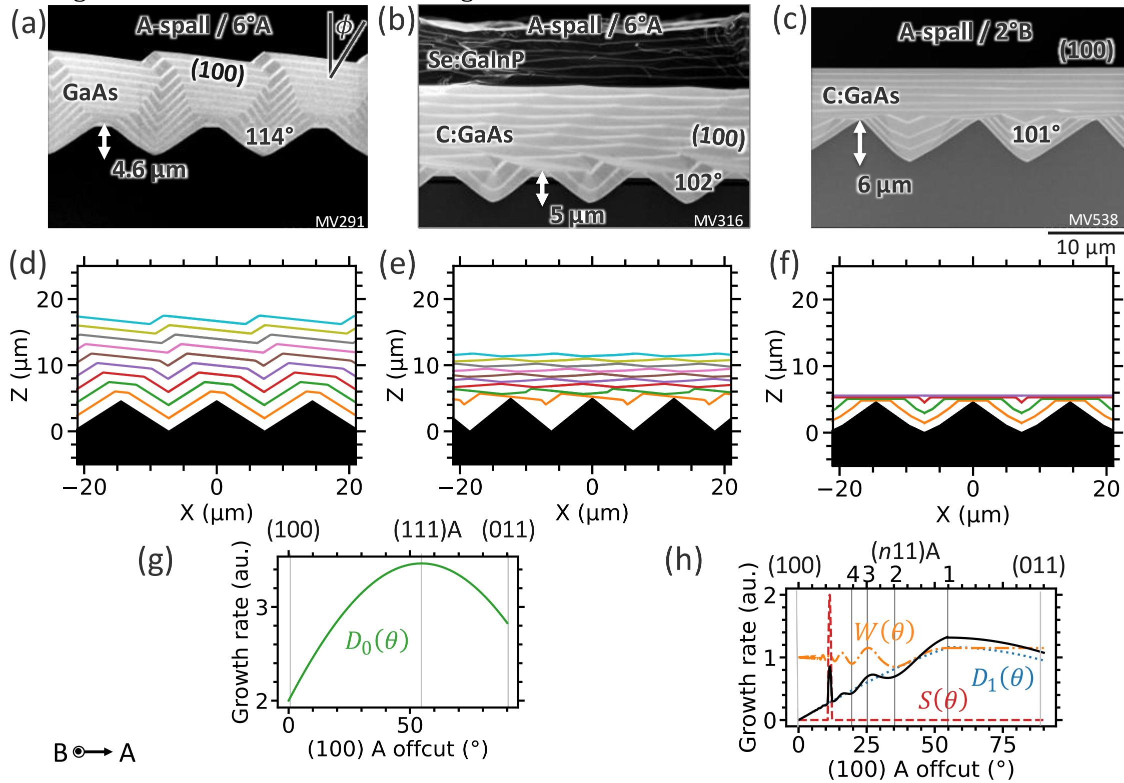


**Figure 6.** Modeling growth morphology. (a-c) Cross-sectional scanning electron microscope images of planarizing GaAs growth on A spalled wafers with (a) 6°A offcut and no $CCl_4$ (recipe M), (b) 6°A offcut and 0.1 sccm $CCl_4$ flow rate (recipe K), and (c) 2°B offcut and 0.1 sccm $CCl_4$ flow rate (recipe M). (d-f) Modeled growth morphology of the surface for the respective images above their positions. We assumed diffusion lengths ($L$) of 3 µm for (d) and 8 µm for (e,f), and growth rates ($R$) according to Eq. 2 with $i = 0$, $C_0 = 0.55, C_1 = C_2 = 0$, and $C_3 = 0.45$ for (d), $i = 1, C_0 = 0.95, C_1 = 4, C_2 = 0.3$, and $C_3 = 0.05$ for (e), and $i = 1, C_0 = 0.9, C_1 = 4, C_2 = 0.3$, and $C_3 = 0.1$ for (f). (g,h) Facet growth rate as a function its angle towards [011] relative the (100) facet, used for the model input parameter ($R(\theta)$). The black curve in (h) represents the $R(\theta)$ function for (f). The darker 6-layer stack grown above the lighter 10-layer stack of C:GaAs in (b) is Se:GaInP with GaAs marker layers.

dangling bond density of As saturated A-facets. However, $D_1(\theta)$ further assumes zero (100) terrace dangling bonds. Additionally, $S(\theta)$ represents a [711]A growth rate spike, while $W(\theta)$ represents a sinusoidal growth rate as a function of $\theta$ with maxima at $(n11)$A facets for $n$-odd. All these functions of $\theta$ (excluding $D_0(\theta)$ ) can serve as proxies for atomic surface reconstructions,[28,29] impacting facet sticking coefficients. Finally, $\cos(\phi)$ is a proxy for gas- or adatom-phase diffusion anisotropy; gas-phase boundary layers may enhance gas flux at the plateau tops versus the sidewalls, and/or adatoms could preferentially diffuse up the sidewalls.[26] The terms' relation with $\theta$ are shown in Figure 6(g,h) and detailed in the Supporting Information.

We find growth for undoped GaAs with recipe M is determined by the surface's unreconstructed dangling bond density and anisotropic Ga diffusion. Qualitatively comparing Figure 6(a) to Figure 6(d), the model matches well with the features observed in the scanning electron microscope cross-section images. Both form (100) plateaus starting at the initial ridge tips and have similar remnant facets. To get this good match, we assume the following fitting parameters for Eq. 2: i=0, $C_0$=0.55, $C_1$=$C_2$=0, $C_3$=0.45. Based on the values of these fitting parameters, the dangling bond density impacts growth rate by 55% with the remaining attributed to anisotropic diffusion, while surface reconstructions have a negligible impact on growth. We also replicate the measured conformal growth of undoped GaAs on a B-faceted surface from a B spall/A offcut substrate with the model, with results in the Supporting Information, and arrive at a similar conclusion.

We observed that introducing a high flow of $CCl_4$ during GaAs growth on A-faceted surfaces altered the physical processes dominating growth. The measured growth morphologies are reproduced with the model, as shown in Figure 6(b,e) and Figure 6(c,f), assuming the following fitting parameters for Eq. 2: i=1, $C_0$=0.9 or 0.95, $C_1$=4, $C_2$=0.3, $C_3$=0.1 or 0.05 for Figure 6(e) and 6(f), respectively. These values suggest that $CCl_4$ or its by-products may be inducing surface reconstructions which significantly impacts growth.

The surface morphology evolution model works well to simulate growth on structured surfaces with sizes less than the Ga-adatom diffusion length as growth follows the relative probabilities of sticking to the facets. However, when only one facet is available, the growth rate instead follows the probability of adatom desorption. Consequently, after planarizing the A spall/2°B offcut sample (Figure 6(c,f)), the model underestimates growth on the (100)2°B facet due to the change in growth mechanism.

## 4. CONCLUSIONS

Reusing GaAs(100) substrates via controlled spalling presents a promising approach to reduce III-V photovoltaic costs; however, the spalling process can create faceted ridges that must be planarized to enable the growth of high-quality photovoltaics.

We grew C:GaAs by MOVPE to planarize A-faceted GaAs(100) substrates, achieving up to 95% material utilization relative to nominal deposition for surface planarization by optimizing the wafer offcut. Introducing a wet etching step to partially planarize the spalled substrate reduced the planarizing growth time to approximately 8 minutes. This time is negligible compared to the 7.5 hours required for the epitaxial growth of high-efficiency solar cells.[30] Additionally, we developed a method to extract adatom diffusion lengths during MOVPE, finding values ranging from 3 to 8 μm for (100) surfaces, depending on the $CCl_4$ gas flow.

Our modeling efforts provided insights into the growth mechanisms, indicating that the slowest growing crystal facet should be perpendicular to the wafer surface normal for optimal planarization. First-principles calculations, as demonstrated by Batyrev et al.,[31] could further explain preferential facet growths and the impacts of surface dopants on atomic surface reconstructions. Coupling these calculations with surface morphology evolution models could enhance their predictive capabilities, allowing for a comprehensive investigation of growth conditions that significantly impact planarization.[16]

The knowledge gained from this study could guide the planarization efforts of other substrate surfaces via epitaxial growth, potentially expanding beyond GaAs(100) substrates. It could also motivate further study of the atomic structure of crystal surfaces during MOVPE growth, given the strong impact on the growth behavior for non-planar surfaces.

**Acknowledgements**
This work was supported by the U.S. Department of Energy under Contract No. DE-AC36-08GO28308 with Alliance for Sustainable Energy, LLC, the Manager and Operator of the National Renewable Energy Laboratory. Funding provided by U.S. Department of Energy, Energy Efficiency and Renewable Energy Solar Energy Technologies Office under Agreement Number 38261. Gavin Forcade was supported by the Natural Sciences and Engineering Research Council of Canada. The U.S. Government retains and the publisher, by accepting the article for publication, acknowledges that the U.S. Government retains a nonexclusive, paid up, irrevocable, worldwide license to publish or reproduce

the published form of this work, or allow others to do so, for U.S. Government purposes.

## REFERENCES


(1) Schulte, K. L.; Johnston, S. W.; Braun, A. K.; Boyer, J. T.; Neumann, A. N.; McMahon, W. E.; Young, M.; Coll, P. G.; Bertoni, M. I.; Warren, E. L.; Steiner, M. A. GaAs Solar Cells Grown on Acoustically Spalled GaAs Substrates with 27% Efficiency. *Joule* **2023**, *7* (7), 1529–1542. https://doi.org/10.1016/j.joule.2023.05.019.

(2) Green, M. A.; Dunlop, E. D.; Siefer, | Gerald; Yoshita, M.; Kopidakis, N.; Bothe, K.; Hao, | Xiaojing. Solar Cell Efficiency Tables (Version 61). *Prog Photovolt* **2022**, *31*, 3–16. https://doi.org/10.1002/pip.3646.

(3) Forcade, G. P.; Valdivia, C. E.; Molesky, S.; Lu, S.; Rodriguez, A. W.; Krich, J. J.; St-Gelais, R.; Hinzer, K. Efficiency-Optimized near-Field Thermophotovoltaics Using InAs and InAsSbP. *Appl. Phys. Lett* **2022**, *121*, 193903. https://doi.org/10.1063/5.0116806.

(4) Amy, C.; Seyf, H. R.; Steiner, M. A.; Friedman, D. J.; Henry, A. Thermal Energy Grid Storage Using Multi-Junction Photovoltaics. *Energy Environ Sci* **2019**, *12* (1), 334–343. https://doi.org/10.1039/c8ee02341g.

(5) Tervo, E. J.; France, R. M.; Friedman, D. J.; Bierman, D. M.; Briggs, J. A.; Steiner, M. A. Efficient and Scalable GaInAs Thermophotovoltaic Devices. *Joule* **2022**, *6*, 1–19. https://doi.org/10.1016/j.joule.2022.10.002.

(6) Beattie, M. N.; Helmers, H.; Forcade, G. P.; Valdivia, C. E.; Hohn, O.; Hinzer, K. InP- and GaAs-Based Photonic Power Converters under O-Band Laser Illumination: Performance Analysis and Comparison. *IEEE J Photovolt* **2023**, *13* (1), 113–121. https://doi.org/10.1109/JPHOTOV.2022.3218938.

(7) Li, J.; Aierken, A.; Liu, Y.; Zhuang, Y.; Yang, X.; Mo, J. H.; Fan, R. K.; Chen, Q. Y.; Zhang, S. Y.; Huang, Y. M.; Zhang, Q. A Brief Review of High Efficiency III-V Solar Cells for Space Application. *Front Phys* **2021**, *8*, 631925. https://doi.org/10.3389/FPHY.2020.631925/BIBTEX.

(8) Horowitz, K. A. W.; Remo, T.; Smith, B.; Ptak, A. *A Techno-Economic Analysis and Cost Reduction Roadmap for III-V Solar Cells*; 2018. https://www.nrel.gov/docs/fy19osti/72103.pdf. (accessed 2023-11-22).

(9) Chen, J.; Packard, C. E. Controlled Spalling-Based Mechanical Substrate Exfoliation for III-V Solar Cells: A Review. *Solar Energy Materials and Solar Cells* **2021**, *225*. https://doi.org/10.1016/j.solmat.2021.111018.

(10) Sweet, C. A.; Schulte, K. L.; Simon, J. D.; Steiner, M. A.; Jain, N.; Young, D. L.; Ptak, A. J.; Packard, C. E. Controlled Exfoliation of (100) GaAs-Based Devices by Spalling Fracture . *Appl. Phys. Lett* **2016**, *108*, 11906. https://doi.org/10.1063/1.4939661.

(11) Mangum, J. S.; Braun, A. K.; Perna, A.; Geisz, J. F.; Ptak, A. J.; Packard, C. E.; France, R. M. Improving Performance of III-V Solar Cells Grown on Spalled Germanium with Ex Situ Substrate Planarization. *Conference Record of the IEEE Photovoltaic Specialists Conference* **2023**. https://doi.org/10.1109/PVSC48320.2023.10359561.

(12) Boyer, J. T.; Braun, A. K.; Schulte, K. L.; Simon, J.; Johnston, S. W.; Guthrey, H. L.; Steiner, M. A.; Packard, C. E.; Ptak, A. J. Analysis of Crystalline Defects Caused by Growth on Partially Planarized Spalled (100) GaAs Substrates. *Crystals 2023, Vol. 13, Page 681* **2023**, *13* (4), 681. https://doi.org/10.3390/CRYST13040681.

(13) Neumann, A. N.; Coll, P. G.; Bertoni, M. I.; Steiner, M. A.; Warren, E. L. Wet-Etching of Acoustically Spalled GaAs for Substrate Reuse. *IEEE J Photovolt* **2024**, *14* (2), 281–287. https://doi.org/10.1109/JPHOTOV.2024.3355405.

(14) Kim, Y.; Park, Y. K.; Kim, M.-S.; Kang, J.-M.; Kim, S.-I.; Hwang, S.-M.; Min, S.-K. Facet Evolution of CCl4-Doped A0.5Ga0.5As/GaAs Multilayers during Metalorganic Chemical Vapor Deposition on Patterned GaAs Substrates. *J Cryst Growth* **1995**, *156*, 169–176.

(15) Braun, A. K.; Boyer, J. T.; Schulte, K. L.; McMahon, W. E.; Simon, J.; Perna, A. N.; Packard, C. E.; Ptak, A. J. 24% Single-Junction GaAs Solar Cell Grown Directly on Growth-Planarized Facets Using Hydride Vapor Phase Epitaxy. *Adv Energy Mater* **2024**, *14* (3), 2302035. https://doi.org/10.1002/AENM.202302035.

(16) McMahon, W. E.; Braun, A. K.; Perna, A. N.; Coll, P. G.; Schulte, K. L.; Boyer, J. T.; Neumann, A. N.; Geisz, J. F.; Warren, E. L.; Ptak, A. J.; Merkle, A. P.; Bertoni, M. I.; Packard, C. E.; Steiner, M. A. In Situ Smoothing of Facets on Spalled GaAs(100) Substrates during OMVPE Growth of III-V Epilayers, Solar Cells, and Other Devices: The Impact of Surface Impurities/Dopants. *Cryst Growth Des* **2024**, *24* (8), 3218–3227. https://doi.org/10.1021/ACS.CGD.3C01407/ASSET/IMAGES/LARGE/CG3C01407_0011.JPEG.

(17) Biasiol, G.; Gustafsson, A.; Leifer, K.; Kapon, E. Mechanisms of Self-Ordering in Nonplanar Epitaxy of Semiconductor Nanostructures. *Phys Rev B* **2002**, *65* (20), 205306. https://doi.org/10.1103/PhysRevB.65.205306.

(18) Hofmann, L.; Knauer, A.; Rechenberg, I.; Zeimer, U.; Weyers, M. Comparison of Binary and Ternary Growth over Trenches Using MOVPE. *J Cryst Growth* **2000**, *213* (3–4), 229–234. https://doi.org/10.1016/S0022-0248(00)00384-5.
(19) Hofmann, L.; Knauer, A.; Rechenberg, I.; Weyers, M. MOVPE Growth of (AlGa)As and (InGa)P on GaAs-Based Trenches. In *26th international symposium on Compound semiconductors*; 1999; pp 75–79.
(20) Kim, S. Il; Kim, M. S.; Kim, Y.; Hwang, S. M.; Min, B. D.; Son, C. S.; Kim, E. K.; Min, S. K. Lateral Growth Rate Control of GaAs on Patterned Substrates by CCl4 and CBr4 during MOCVD. *J Cryst Growth* **1997**, *170* (1–4), 665–668. https://doi.org/10.1016/S0022-0248(96)00572-6.
(21) Ohtsuka, M.; Miyazawa, S. Model for Molecular-Beam-Epitaxy Growth over Nonplanar Surfaces. *J Appl Phys* **1988**, *64* (7), 3522–3527. https://doi.org/10.1063/1.341490.
(22) Soci, C.; Bao, X. Y.; Aplin, D. P. R.; Wang, D. A Systematic Study on the Growth of GaAs Nanowires by Metal-Organic Chemical Vapor Deposition. *Nano Lett* **2008**, *8* (12), 4275–4282. https://doi.org/10.1021/NL801986R/SUPPL_FILE/NL801986R_SI_001.PDF.
(23) Liu, Y.; Shimomura, S.; Sano, N.; Garno, K.; Adachi, A.; Hiyamizu, S. Improved GaAs/AIAs Multilayer Structures Grown by MBE on Patterned GaAs (100) Substrates with Ridges along the [011] Direction. *Semicond. Sci. Technoi* **1993**, *8*, 2197–2200.
(24) López, M.; Nomura, Y. Surface Diffusion Length of Ga Adatoms in Molecular-Beam Epitaxy on GaAs(100)–(110) Facet Structures. *J Cryst Growth* **1995**, *150*, 68–72. https://doi.org/10.1016/0022-0248(95)80182-C.
(25) Rondanini, M.; Cavallotti, C.; Moscatelli, D.; Masi, M.; Carrà, S. A Combined Fluid Dynamic and 3D Kinetic Monte Carlo Investigation of the Selective Deposition of GaAs and InP. *J Cryst Growth* **2004**, *272* (1–4), 52–58. https://doi.org/10.1016/J.JCRYSGRO.2004.08.051.
(26) Mao, H.; Jing, W.; Wang, J.; Yu, J.; Wang, L.; Dai, N. Nucleation and Growth Mechanism of GaAs Epitaxial Growth. *Thin Solid Films* **2007**, *515* (7–8), 3624–3628. https://doi.org/10.1016/J.TSF.2006.10.015.
(27) Kim, H. J.; Park, Y. K.; Kim, S.-I.; Kim, E. K.; Kim, T. W. Facet Evolution of Al 0.5 Ga 0.5 As/GaAs Multilayers Grown on Mesa-Patterned GaAs Substrate. *Jpn J Appl Phys* **1999**, *38* (9A), 4969–4972.
(28) Xue, Q. K.; Hashizume, T.; Sakurai, T. Scanning Tunneling Microscopy of III-V Compound Semiconductor (001) Surfaces. *Prog Surf Sci* **1997**, *56* (1–2), 1–131. https://doi.org/10.1016/S0079-6816(97)00033-6.
(29) Li, L.; Qi, H.; Gan, S.; Han, B.-K.; Hicks, R. F. Site-Specific Chemistry of Carbon Tetrachloride Decomposition on GaAs(001). *Appl. Phys. A* **1998**, *66*, 501–505.
(30) John F. Geisz; Ryan M. France; Kevin L. Schulte; Myles A. Steiner; Andrew G. Norman; Harvey L. Guthrey; Matthew R. Young; Tao Song; Thomas Moriarty. Six-Junction III–V Solar Cells with 47.1% Conversion Efficiency under 143 Suns Concentration. *Nat Energy* **2020**, *5*, 326–335.
(31) Batyrev, I. G.; McMahon, W. E.; Zhang, S. B.; Olson, J. M.; Wei, S.-H. Step Structures on III-V Phosphide (001) Surfaces: How Do Steps and Sb Affect CuPt Ordering of GaInP? *Phys Rev Lett* **2005**, *94*, 096101. https://doi.org/10.1103/PhysRevLett.94.096101.